Myostatin Augments Muscle-Specific Ring Finger Protein-1 Expression Through an NF-kB Independent Mechanism in SMAD3 Null Muscle

Sandhya Sriram, Subha Subramanian, Prasanna Kumar Juvvuna, Xiaojia Ge, Sudarsanareddy Lokireddy, Craig Desmond McFarlane, Walter Wahli, Ravi Kambadur, and Mridula Sharma

Division of Molecular Genetics and Cell Biology (S.Sr., S.Su., R.K.), School of Biological Sciences, Nanyang Technological University, Singapore 637551; Department of Biochemistry (P.K.J., M.S.) YLLSoM, National University of Singapore, MD6, Level 14 S Core, Singapore 117599; Growth, Development and Metabolism Program (X.G., C.D.M., R.K.), Singapore Institute of Clinical Sciences, Brenner Centre for Molecular Medicine, Singapore 117609; Department of Cell Biology (S.L.), Harvard Medical School, Boston, Massachusetts 02115-5730; and Center for Integrative Genomics (W.W.), University of Lausanne, Lausanne, Switzerland

Smad (Sma and Mad-related protein) 2/3 are downstream signaling molecules for TGF-β and myostatin (Mstn). Recently, Mstn was shown to induce reactive oxygen species (ROS) in skeletal muscle via canonical Smad3, nuclear factor-κB, and TNF-α pathway. However, mice lacking Smad3 display skeletal muscle atrophy due to increased Mstn levels. Hence, our aims were first to investigate whether Mstn induced muscle atrophy in Smad3$^{-/-}$ mice by increasing ROS and second to delineate Smad3-independent signaling mechanism for Mstn-induced ROS. Herein we show that Smad3$^{-/-}$ mice have increased ROS levels in skeletal muscle, and inactivation of Mstn in these mice partially ablates the oxidative stress. Furthermore, ROS induction by Mstn in Smad3$^{-/-}$ muscle was not via nuclear factor-κB (p65) signaling but due to activated p38, ERK MAPK signaling and enhanced IL-6 levels. Consequently, TNF-α, nicotinamide adenine dinucleotide phosphate oxidase, and xanthine oxidase levels were up-regulated, which led to an increase in ROS production in Smad3$^{-/-}$ skeletal muscle. The exaggerated ROS in the Smad3$^{-/-}$ muscle potentiated binding of C/EBP homology protein transcription factor to *MuRF1* promoter, resulting in enhanced MuRF1 levels leading to muscle atrophy. **(*Molecular Endocrinology* 28: 317–330, 2014)**

Smads (Sma and Mad-related proteins) are a family of intracellular proteins that transduce extracellular signals from TGF-β superfamily members (1, 2). Upon TGF-β ligand binding and subsequent receptor activation, Smad2 and Smad3 get phosphorylated to form a complex with the common mediator Smad4. The Smad2/3-Smad4 complex then translocates into the nucleus to activate or repress the transcription of TGF-β target genes. Several reports have indicated that disruption of TGF-β and/or the Smad signaling pathway is causal to the pathogenesis of several disorders (3, 4) and fibrogenesis (5).

Myostatin (Mstn), a member of the TGF-β superfamily signals predominantly through the Smad2/3 pathway to inhibit myogenesis (6, 7). Specifically, Smad3 is required by Mstn to inhibit differentiation of myoblasts (8) and to activate proliferation of fibroblasts (9). In addition, Smad3-dependent mechanisms of Mstn-mediated muscle wasting have been described (10, 11). Mstn has also been shown to induce reactive oxygen species (ROS)

ISSN Print 0888-8809 ISSN Online 1944-9917
Printed in U.S.A.

Received June 13, 2013. Accepted January 13, 2014.
First Published Online January 17, 2014

Abbreviations: AOE, antioxidant enzyme; CAT, catalase; CCM, control conditioned medium; ChIP, chromatin immunoprecipitation; CHO, Chinese hamster ovary; CHOP, C/EBP homology protein; CMM, conditioned medium containing Mstn; ETC, electron transport chain; GPx, glutathione peroxidase; GSR, reduced glutathione; JNK, c-Jun N-terminal kinase; KO, knockout; mETC, mitochondrial ETC; RT-qPCR, reverse transcriptase-quantitative PCR; Smad, Sma and Mad-related protein; SIS3, specific inhibitor of Smad3; SOD, super oxide dismutase; TAK1, TGF-β-activated kinase 1; WT, wild type; XO, xanthine oxidase.

through canonical Smad2/3, nuclear factor-κB (NF-κB), TNF-α, and nicotinamide adenine dinucleotide phosphate oxidase 1 (*Nox1*) signaling to target muscle-specific E3 ligases, MuRF1, and Atrogin1 in skeletal muscle (12). Recently, elevated levels of Mstn in the absence of Smad3 were reported to contribute to the muscle atrophy and regeneration defects observed in Smad3$^{-/-}$ mice (13, 14), indicating that Mstn was signaling muscle atrophy through Smad3-independent mechanisms. In an earlier report, Mstn was found to activate p38 MAPK to upregulate p21 and inhibit myoblast proliferation (15). Likewise, Mstn activated the ERK1/2 pathway to inhibit muscle cell differentiation and growth (16). However, the alternative Mstn signaling mechanisms in the absence of canonical Smad3 signaling leading to muscle atrophy are not fully known.

Given the fact that Mstn levels are elevated in Smad3$^{-/-}$ mice and that Mstn also acts as a pro-oxidant, we investigated the Smad3-independent mechanisms by which Mstn induced muscle atrophy in Smad3$^{-/-}$ muscle. Using in vitro and in vivo approaches herein we show that Smad3 was required for Mstn-mediated induction of ROS via NF-κB (p65) signaling. Furthermore, the results demonstrate that Mstn induced ROS through p38 and ERK MAPK pathways mediated through IL-6, TNF-α, Nox, and xanthine oxidase (XO) in Smad3$^{-/-}$ mice. The excessive oxidative stress thus resulted in enhanced binding of C/EBP homology protein (CHOP), a transcription factor induced by cellular oxidative stress, to *MuRF1* promoter in Smad3$^{-/-}$ muscle. Finally, increased protein degradation by MuRF1 would result in muscle atrophy.

Materials and Methods

Animals

Smad3$^{-/-}$ mice and Mstn$^{-/-}$ mice were obtained as previously described (12, 13). The double-knockout (KO) mice (Smad3$^{-/-}$/Mstn$^{-/-}$) were generated and genotyped according to previously published protocol (13). C57Bl/6J mice (wild type [WT]) were obtained from National University of Singapore-Centre for Animal Resources, Singapore. All mice used in this study were 6-week-old females maintained at Nanyang Technological University Animal house, Singapore. All experimental procedures were approved by the Institutional Animal Care and Use Committee, Singapore.

Reagents and proteins

The Mstn expressing Chinese hamster ovary (CHO) cell line was used to obtain Mstn protein containing conditioned medium (17); denoted as CMM in this manuscript. Enzyme Immuno Assay (Immundiagnostik AG) was used to determine the concentration of Mstn in the conditioned medium. The supplemental data include the list of various reagents and chemicals used in the current study.

Isolation of primary myoblasts (satellite cells)

The hind limb skeletal muscles from WT and Smad3$^{-/-}$ mice were dissected and used for isolation of primary myoblasts. Primary myoblasts were isolated according to the previously described protocol (18, 19).

Cell culture

Established American Type Culture Collection murine C2C12 myoblast cell line was used (20). Stable shSmad3 and shControl C2C12 cells were established as previously described (13). The myoblasts were passaged in proliferation medium (DMEM [PAA Laboratories, Inc], 10% fetal bovine serum [HyClone Laboratories, Inc], 1% Penicillin/Streptomycin [Gibco]) and differentiated in differentiation medium (DMEM, 2% horse serum (Gibco), 1% Penicillin/Streptomycin). The stable cell lines were passaged in proliferation medium containing puromycin and differentiated in puromycin containing differentiation medium.

Treatment of C2C12, shSmad3, and shControl C2C12 cells

The concentration of Mstn in conditioned medium from CHO cells (CMM) used in all the experiments was 3.5 ng/mL. This concentration was used to treat C2C12 cells, shSmad3, and shControl C2C12 cells during differentiation. Equal volume of control conditioned medium from CHO cells (CCM) was used, which served as the control in all experiments. Based on earlier studies, 10 μM/mL specific inhibitor of Smad3 (SIS3) (21), 10 μM/mL SB203580 (22), and 10 μM/mL U0126 (23) were used to treat C2C12, shSmad3, and shControl C2C12 cells during differentiation.

RT-qPCR (reverse transcriptase-quantitative PCR)

WT and Smad3$^{-/-}$ primary myoblasts as well as shSmad3 and shControl C2C12 cells treated with inhibitors and CCM or CMM were harvested and suspended in TRIZOL (Invitrogen) for RNA isolation. RNA was also isolated from Gastrocnemius muscle of WT, Smad3$^{-/-}$, Mstn$^{-/-}$, and double-KO mice using TRIZOL, as per the manufacturer's protocol (Invitrogen). The RT-qPCR was performed exactly as explained previously (12). The forward and reverse primers used are given in Supplemental Table 1 published on The Endocrine Society's Journals Online web site at http://mend.endojournals.org.

Analysis of ROS production

Intracellular visualization of ROS

ROS production was assayed in differentiating WT and Smad3$^{-/-}$ primary myoblasts using the fluorescent dye, CM-H2DCFDA, as described previously (12).

Analysis of components of signaling pathways and the enzymes involved in ROS generation in Smad3$^{-/-}$ myoblasts

The cell-signaling inhibitors used in this study were according to Iuchi et al (24). WT and Smad3$^{-/-}$ primary myoblasts

were treated with the inhibitors as described previously (12); however the myoblasts were not treated with Mstn. ROS production was assayed using the fluorescent dye, CM-H2DCFDA, as described previously (12).

Protein isolation

WT and Smad3$^{-/-}$ primary myoblasts, shSmad3, and shControl C2C12 cells subjected to various treatments with inhibitors and CMM during differentiation were collected at indicated time points in protein lysis buffer. Protein lysates were subsequently made as previously described (12). Gastrocnemius muscle from WT, Smad3$^{-/-}$, Mstn$^{-/-}$, and double-KO mice were homogenized in protein lysis buffer, and the clear supernatants were collected. Cytoplasmic and nuclear fractions from biceps femoris muscle and cells following various treatments were isolated as previously described (25). The protein concentrations were measured by Bradford's assay (26).

Western blot analysis

Total protein, nuclear, and cytoplasmic extracts (20–30 μg) were separated on 4%–12% Bis-Tris polyacrylamide gels (Invitrogen) and transferred to nitrocellulose membrane by electroblotting. The membranes were blocked and probed with specific primary antibodies, followed by incubation with respective secondary antibodies (Supplemental Table 2). Horseradish peroxidase activity was detected using Western Lightning Plus Enhanced Chemiluminescence (PerkinElmer).

Oxyblot assay

To estimate carbonyl groups incorporated into proteins by oxidation due to ROS, Oxyblot assay was performed according to the manufacturers' instructions using the Oxyblot Protein Oxidation Detection Kit (Millipore Corp).

Cell and muscle homogenates for enzyme assays

The cell homogenates from WT and Smad3$^{-/-}$ primary myoblasts and muscle homogenates of quadriceps muscles were made according to Sriram et al (12) except that the cells were not treated with Mstn. The protein concentrations of the cell lysates and muscle homogenates were measured by Bradford's assay (26).

Xanthine oxidase (XO) assay

XO activity was measured in primary myoblast lysates and in muscle homogenates using a continuous spectrophotometric rate determination assay as described by Bergmeyer (27).

Antioxidant enzyme activity-super oxide dismutase (SOD), catalase (CAT), and glutathione peroxidase (GPx)

The activity of SOD was estimated as previously described (12). The method of Beers and Sizer (28) was used to assay catalase activity. Glutathione peroxidase enzyme assay was performed by the modified method of Rotruck et al (29) as described previously (12).

Antioxidant-reduced glutathione (GSR) estimation

The total reduced glutathione was measured by the method of Moron et al (30).

EMSA

The oligonucleotides containing the CHOP binding site on mouse *MuRF1* promoter (5′-AAAGTCTCAGTGCAATGCG-CAGCCCATAA-3′) were hybridized to their respective complementary strands and labeled at the 3′-end with Biotin Tetraethyleneglycol (Sigma-Aldrich). The EMSAs were performed using the Lightshift Chemiluminescent EMSA kit (Thermo Scientific). Nuclear extracts (4 μg) obtained from biceps femoris muscles were incubated with the biotin-labeled probe (final concentration 1 nM (1×)), and EMSA was performed as previously described (12). Unlabeled probes were used as competitors at concentrations 500 nM (500 ×). To confirm specificity of CHOP binding, 4 μL of CHOP antibody was added to the nuclear extract and preincubated for 20 minutes at room temperature before incubation with the labeled probe.

Chromatin immunoprecipitation (ChIP) assay

C2C12 myoblasts were treated with SIS3 for 48 hours during differentiation. ChIP assay was performed according to the published protocol (31). The protocol is briefly explained in Supplemental *Materials and Methods*. The following set of primers was used for PCR: *Chop* forward (F) primer, 5′-AAGCAGGT-GCCACTCTCTGT-3′; and *Chop* reverse (R) primer, 5′-GTAGCTGATTTGGCCCATGT-3′.

Plasmids

Murine CHOP full-length cDNA was amplified using KAPA Taq Hotstart Polymerase kit (KAPA Biosystems, Inc). The F and R primers containing *Hin*dIII and *Xho*I restriction enzyme sequences used for PCR are F, 5′-AAGCTTACGTGCAGT-CATGGCAGCTG-3′; and R, 5′-CTCGAGGCCCACTGTT CATGCTTGGT-3′, respectively. The PCR product was then cloned into pGEM-T Easy vector (Promega Corp) and subsequently into *Hin*dIII and *Xho*I sites of pcDNA3 expression vector. The expression of CHOP protein was confirmed by Western blot analysis on protein lysates obtained from C2C12 cells transfected with pcDNA3-CHOP vector.

The mouse *MuRF1* promoter (~4,000 bp) was obtained by PCR using bacterial artificial chromosome clone RP23–40E12 (Children's Hospital Oakland Research Institute). The primer sequences are, F, 5′-CTCGAGCCAAGCCCATTAGTGCA-GATC-3′; and R, 5′-AAGCTTCACTCGGATCCTCTTTGT CTTCGTC-3′, and PCR was performed using Q5 Hot Start High-Fidelity DNA Polymerase (New England Biolabs Inc) according to the manufacturer's instructions followed by A-tailing. The PCR product was cloned into pGEM-T Easy vector and sequenced and then subcloned into *Xho*1 and *Hin*dIII sites of pGL4.10 vector (Promega Corp) to generate pGL4.10-MuRF1P.

Luciferase assay

C2C12 myoblasts were plated at a density of 10 000 cells/cm^2 in 6-well plates. Following overnight attachment, the C2C12 myoblasts were transfected in triplicate with either pGL4.10 and pcDNA3 empty vectors or pGL4.10-MuRF1promoter (pGL4.10-MuRF1P) and pcDNA3 or pGL4.10-MuRF1P and pcDNA3-CHOP, together with the control *Renilla* luciferase vector pRL-TK using Lipofectamine 2000 (Invitrogen), as per the manufacturer's guidelines. Next day the medium was replaced with differentiation medium and the

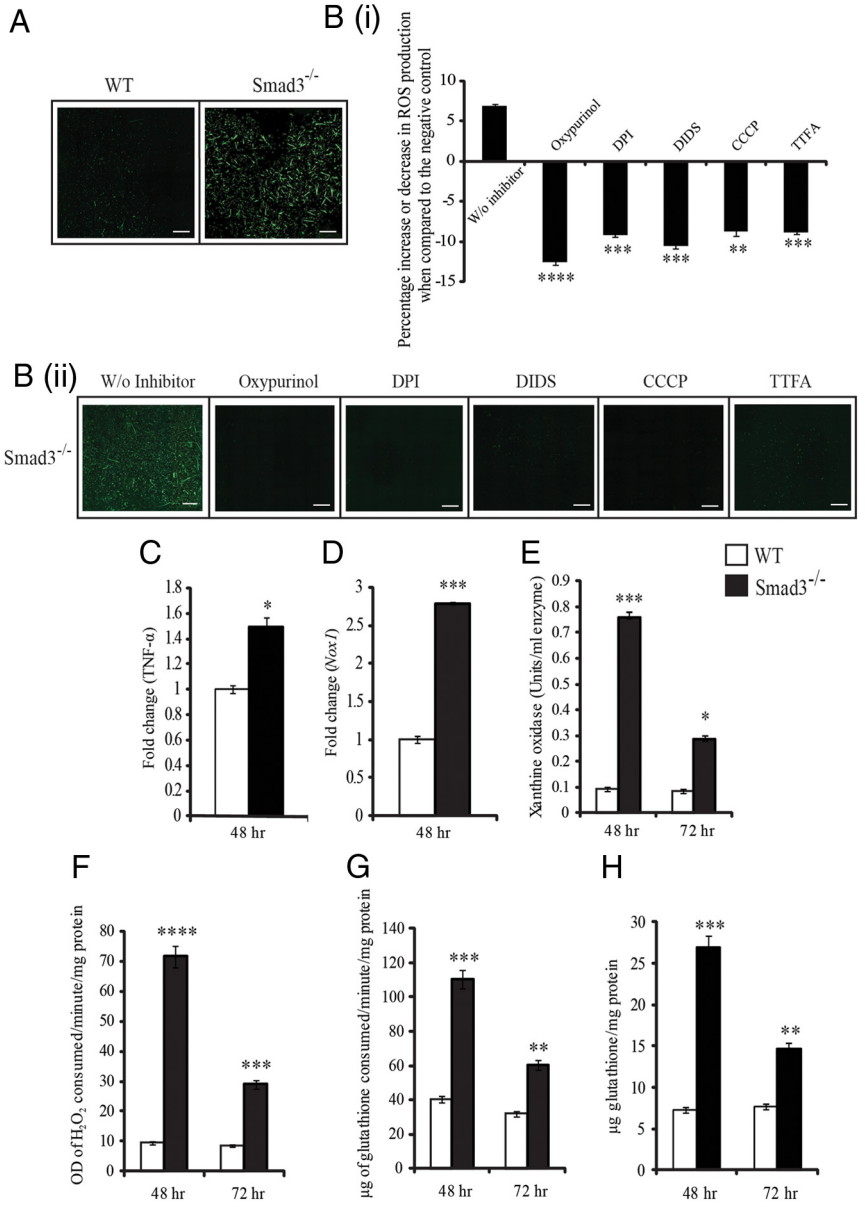

Figure 1. Smad3$^{-/-}$ myoblasts have increased ROS production and AOE activity. A, Representative images showing ROS production at 48 hours during differentiation in WT and Smad3$^{-/-}$ primary myoblasts, probed with the CM-H2DCFDA fluorescent probe. The images were taken using a Leica upright microscope at ×10 magnification. Increased fluorescence (green) intensity is directly proportional to increased ROS production in myoblasts. Scale bar, 100 μm (n = 3). B (i), Smad3$^{-/-}$ primary myoblasts were treated for 48 hours during differentiation in the presence of ROS cell signaling inhibitors and ROS content was measured using the CM-H2DCFDA probe using a fluorescent multilabel plate reader. The data are expressed as percentage increase or decrease in ROS production; **, $P < .01$; ***, $P < .001$; ****, $P < .0001$ (n = 3). B (ii), ROS production in Smad3$^{-/-}$ primary myoblasts treated for 48 hours during differentiation in the presence of ROS cell signaling inhibitors using the CM-H2DCFDA probe. The fluorescence was viewed as mentioned in panel A. Scale bar, 100 μm (n = 3). mRNA expression of TNF-α (C) and *Nox1* (D) in WT and Smad3$^{-/-}$ primary myoblasts in differentiation medium for 48 hours. *, $P < .05$; ***, $P < .001$ (n = 3). XO production assay (E) and enzyme assays for CAT (F), GPx (G) and GSR (H) were performed on protein lysates from differentiating WT and Smad3$^{-/-}$ primary myoblasts at indicated time points. *, $P < .05$; **, $P < .01$; ***, $P < .001$; ****. $P < .0001$ (n = 3).

myoblasts were incubated for a further 48 hours. Luciferase assays were performed using the Dual Luciferase Assay System, as per the manufacturer's protocol (Promega Corp). Relative luciferase activity in each of the extracted protein samples was measured in triplicate using the Fluoroskan Ascent Microplate Fluorometer and Luminometer (Thermo Fisher Scientific, Inc).

Statistical analysis

The *P* value was calculated using ANOVA and Student's *t* test with $P < .05$ being considered as significant. Three mice per genotype were used for various experiments. Results are presented as mean ± SE of 2 or 3 independent experiments.

Results

Smad3$^{-/-}$ myoblasts have increased ROS production

Smad3$^{-/-}$ mice were shown to have impaired myoblast proliferation and differentiation resulting in pronounced skeletal muscle atrophy (13). The mRNA expression of *Mstn*, a candidate gene that regulates muscle atrophy, was up-regulated in skeletal muscle of Smad3$^{-/-}$ mice (13). Recently, it has been shown that Mstn is a pro-oxidant and induces the production of ROS in myoblasts (12). Hence, to investigate whether the elevated *Mstn* expression in Smad3$^{-/-}$ mice is associated with increased ROS production, we measured ROS levels in differentiating myoblasts of WT and Smad3$^{-/-}$ mice using the fluorescent dye, CM-H2DCFDA (Molecular Probes). The results show that ROS production was increased in Smad3$^{-/-}$ myoblasts when compared with the WT myoblasts, as shown by the increased fluorescence in the Smad3$^{-/-}$ myoblasts (Figure 1A).

ROS in Smad3$^{-/-}$ myoblasts is produced by mitochondrial electron transport chain (mETC) and XO

In order to understand the mechanism behind ROS production in Smad3$^{-/-}$ myoblasts, cell signaling inhibitors (Sigma-Aldrich) that inhibit various enzymes and pathways involved in ROS production

were used (24). Diphenylene iodinium chloride (DPI) (inhibitor of Nox and Complex I of mETC), 4, 4′-diisothiocyanatostilbene-2, 2′-disulfonic acid disodium salt (DIDS) (inhibitor of superoxide release from mitochondria), carbonyl cyanide 3-chlorophenylhydrazone (CCCP) (inhibitor of mitochondrial membrane proton gradient), and 2-thenoyltrifluoroacetone (TTFA) (inhibitor of complex II of mETC) block ROS production by Nox and mETC, which have already been shown to be sources of ROS induced by Mstn (12). Similarly in Smad3$^{-/-}$ mice, these inhibitor treatments revealed that ROS was predominantly produced by Nox and mETC (Figure 1B(i) and 1B(ii)). In addition, treatment with Oxypurinol (inhibitor of XO) inhibited ROS production in Smad3$^{-/-}$ myoblasts (Figure 1B(i) and 1B(ii)), indicating that XO, another important enzyme that contributes to the generation of ROS is involved in the induction of oxidative stress in Smad3$^{-/-}$ mice.

Our laboratory showed that Mstn induces ROS via TNF-α and Nox in skeletal muscle. Hence, RT-qPCR for TNF-α and *Nox1* was performed in differentiating WT and Smad3$^{-/-}$ primary myoblasts. The results showed that TNF-α (Figure 1C) and *Nox1* (Figure 1D) expression was increased in Smad3$^{-/-}$ primary myoblasts during differentiation. Because our results indicate that XO also produces ROS in Smad3$^{-/-}$ myoblasts, an XO assay was performed in protein lysates from differentiating WT and Smad3$^{-/-}$ primary myoblasts. The results showed significantly increased XO activity in Smad3$^{-/-}$ myoblasts during differentiation (Figure 1E). These results indicate that ROS is produced in Smad3$^{-/-}$ muscle cells by TNF-α, Nox, and also by XO.

Smad3$^{-/-}$ myoblasts have increased antioxidant enzyme (AOE) activity

An important marker for oxidative stress is AOE production, which is enhanced in cells in response to elevated ROS. As it has already been shown in our previous study that Mstn induces AOE activity (12), we decided to determine the antioxidant status of Smad3$^{-/-}$ myoblasts. Thus, the activities of the enzymatic antioxidants, CAT and GPx, and level of nonenzymatic antioxidant, GSR, were measured in differentiating WT and Smad3$^{-/-}$ primary myoblasts. Increased activity of CAT (Figure 1F) and GPx (Figure 1G) was observed in Smad3$^{-/-}$ myoblasts, together with increased GSR levels (Figure 1H). These data indicate that the increased ROS in Smad3$^{-/-}$ myoblasts, potentially induced by Mstn, results in the production of AOEs and GSR.

Loss of Mstn relieves oxidative stress in Smad3$^{-/-}$ muscle

It has been recently shown that genetic inactivation of Mstn in Smad3$^{-/-}$ mice (double-KO mice), partially alleviates muscle atrophy (13). Because Smad3$^{-/-}$ myoblasts demonstrated increased ROS production and elevated Mstn levels, we used double-KO mice to test whether the loss of Mstn is able to reduce the oxidative stress in Smad3$^{-/-}$ mice. First, we analyzed the protein carbonylation, a standard marker for oxidative stress, in gastrocnemius muscle of WT, Smad3$^{-/-}$, Mstn$^{-/-}$, and double-KO mice by immunoblotting, using an anti-DNP antibody (Millipore Corp) (Figure 2A(i)). Densitometric analysis (Figure 2A(ii)) of the oxyblot revealed that while Smad3$^{-/-}$ muscle had significantly higher levels of carbonylated proteins, Mstn$^{-/-}$ muscle had significantly lower levels of carbonylated proteins, when compared with WT muscle. Furthermore, the level of protein carbonylation in the double-KO muscle was similar to that observed in WT muscle, suggesting that inactivation of Mstn ameliorates the effect of the enhanced ROS production observed in Smad3$^{-/-}$ muscle.

Next, the mRNA expression of TNF-α and *Nox1* was analyzed in gastrocnemius muscle of WT, Smad3$^{-/-}$, Mstn$^{-/-}$, and double-KO mice. The results indicate that Smad3$^{-/-}$ muscle had significantly up-regulated expression of TNF-α (Figure 2B) and *Nox1* (Figure 2C) when compared with WT muscle; whereas in double-KO muscle, the expression of TNF-α (Figure 2B) and *Nox1* (Figure 2C) was similar to that observed in WT muscle and significantly down-regulated when compared with Smad3$^{-/-}$ muscle. The enzyme activity of XO was also assayed in the muscle tissue, and results indicated that Smad3$^{-/-}$ muscle has higher XO activity when compared with WT, Mstn$^{-/-}$, and double-KO muscle tissues (Figure 2D).

Further, the effect of inactivation of Mstn on the basal activities of AOEs and nonenzymatic antioxidants in double-KO mice was determined. The results revealed that Smad3$^{-/-}$ muscle had significantly increased SOD activity (Figure 2E) and GSR (Figure 2F) level when compared with the WT muscle, whereas the double-KO muscle had the lowest SOD activity when compared with WT, Smad3$^{-/-}$, and Mstn$^{-/-}$ muscle (Figure 2E). The level of GSR in double-KO muscle was similar to that of WT muscle and significantly lower when compared with Smad3$^{-/-}$ muscle (Figure 2F). These findings confirm that inactivation of Mstn in Smad3$^{-/-}$ mice helps to maintain basal AOE activity in skeletal muscle.

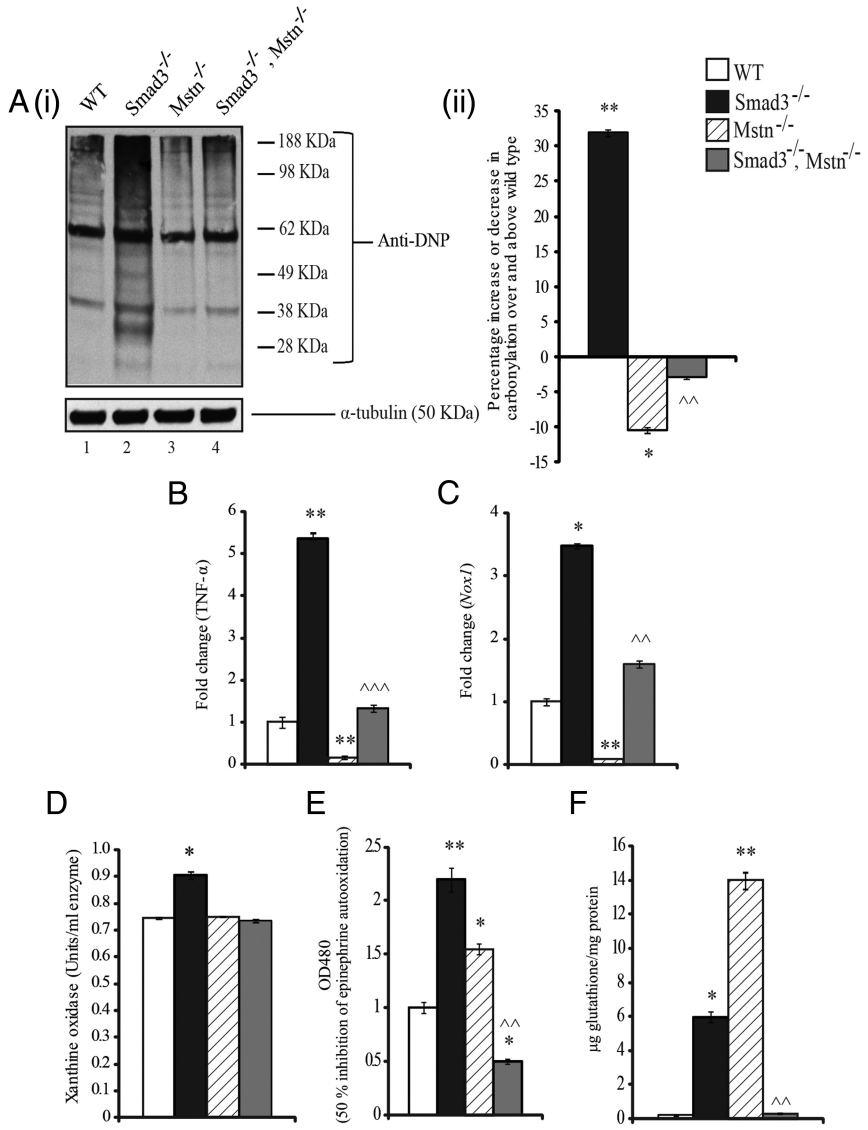

Figure 2. Loss of Mstn relieves oxidative stress in Smad3$^{-/-}$ muscle. A (i), Representative gel showing protein carbonylation in protein lysates of gastrocnemius muscle from WT, Smad3$^{-/-}$, Mstn$^{-/-}$. and double-KO mice as detected using the Oxyblot assay kit. A (ii), Corresponding densitometric analysis of the gel showing the percentage increase or decrease in carbonylation over and above WT muscle (*, $P < .05$; **, $P < .01$); ^^, $P < .01$: double-KO muscle as compared with Smad3$^{-/-}$ muscle. α-Tubulin was used as an internal control for equal protein loading on the gel (n = 3). Representative graph showing mRNA expression of TNF-α (B) and *Nox1* (C) in gastrocnemius muscle from WT, Smad3$^{-/-}$, Mstn$^{-/-}$, and double-KO mice. *, $P < .05$; **, $P < .01$: when compared with the WT muscle; ^^, $P < .01$; ^^^, $P < .001$: when compared to Smad3$^{-/-}$ muscle (n = 3). Representative graph showing enzyme assays for XO (D), SOD (E), and GSR (F) performed on whole-muscle lysates of quadriceps muscle from WT, Smad3$^{-/-}$, Mstn$^{-/-}$, and double-KO mice. *, $P < .05$; **, $P < .01$: when compared with the WT muscle; ^^, $P < .01$: when compared to Smad3$^{-/-}$ muscle (n = 3).

Smad3 is required for activation of NF-κB (p65) by Mstn

Recently, it has been shown that Mstn signals through NF-κB to induce ROS in skeletal muscle cells (12). Hence, whole-muscle lysates, and nuclear and cytoplasmic extracts of Biceps femoris muscle from WT, Smad3$^{-/-}$, Mstn$^{-/-}$, and double-KO mice were analyzed by Western blot to assess the levels of proteins involved in NF-κB signaling (Figure 3A(i), (ii), (iii), and (iv)). No change in the level of NF-κB (p65) protein was observed in whole-muscle lysates collected from Smad3$^{-/-}$ (lane 2) and double-KO mice (lane 4), when compared with WT mice (lane 1); however, a decrease in NF-κB (p65) level was observed in Mstn$^{-/-}$ mice (lane 3), a feature consistent with previously published work (12). A significant decrease in NF-κB (p65) levels was detected in both cytoplasmic and nuclear extracts of Smad3$^{-/-}$ (lane 2), Mstn$^{-/-}$ (lane 3), and double-KO (lane 4) muscle when compared with WT muscle (lane 1) (Figure 3A(i)). The level of p-NF-κB (p65) in the nuclear extract of Smad3$^{-/-}$ (lane 2), Mstn$^{-/-}$ (lane 3), and double-KO (lane 4) muscle was significantly lower than that detected in WT muscle (lane 1) (Figure 3A(i) and (ii)). The level of p-IκB-α (Figure 3A(i) and (iii)) was reduced in Smad3$^{-/-}$ (lane 2), Mstn$^{-/-}$ (lane 3), and double-KO (lane 4) cytoplasmic extracts, whereas reduced IκB-α levels were detected in the cytoplasmic extract from Smad3$^{-/-}$ muscle (lane 2), when compared with WT muscle (lane 1). IKKα levels were also significantly decreased in Smad3$^{-/-}$ (lane 2), Mstn$^{-/-}$ (lane 3), and double-KO (lane 4) cytoplasmic extracts (Figure 3A(i) and (iv)). Taken together, these results indicate that loss of Smad3 does not result in aberrant activation of NF-κB signaling and moreover, because Mstn levels are enhanced in Smad3$^{-/-}$ mice, we propose that Smad3 may be required for Mstn-mediated activation of NF-κB.

To confirm this hypothesis, C2C12 cells were treated with SIS3 (Sigma-Aldrich), a specific inhibitor of Smad3, in the absence or presence of CMM during differentiation. Western blot analysis was performed to assess the protein levels of NF-κB (p65), p-NF-κB (p65), p-IκB-α, IκB-α, and IKKα in whole-cell lysates and nuclear and cytoplasmic extracts obtained from treated C2C12 cells. As expected, treatment with CMM resulted in activation of NF-κB (p65) signaling

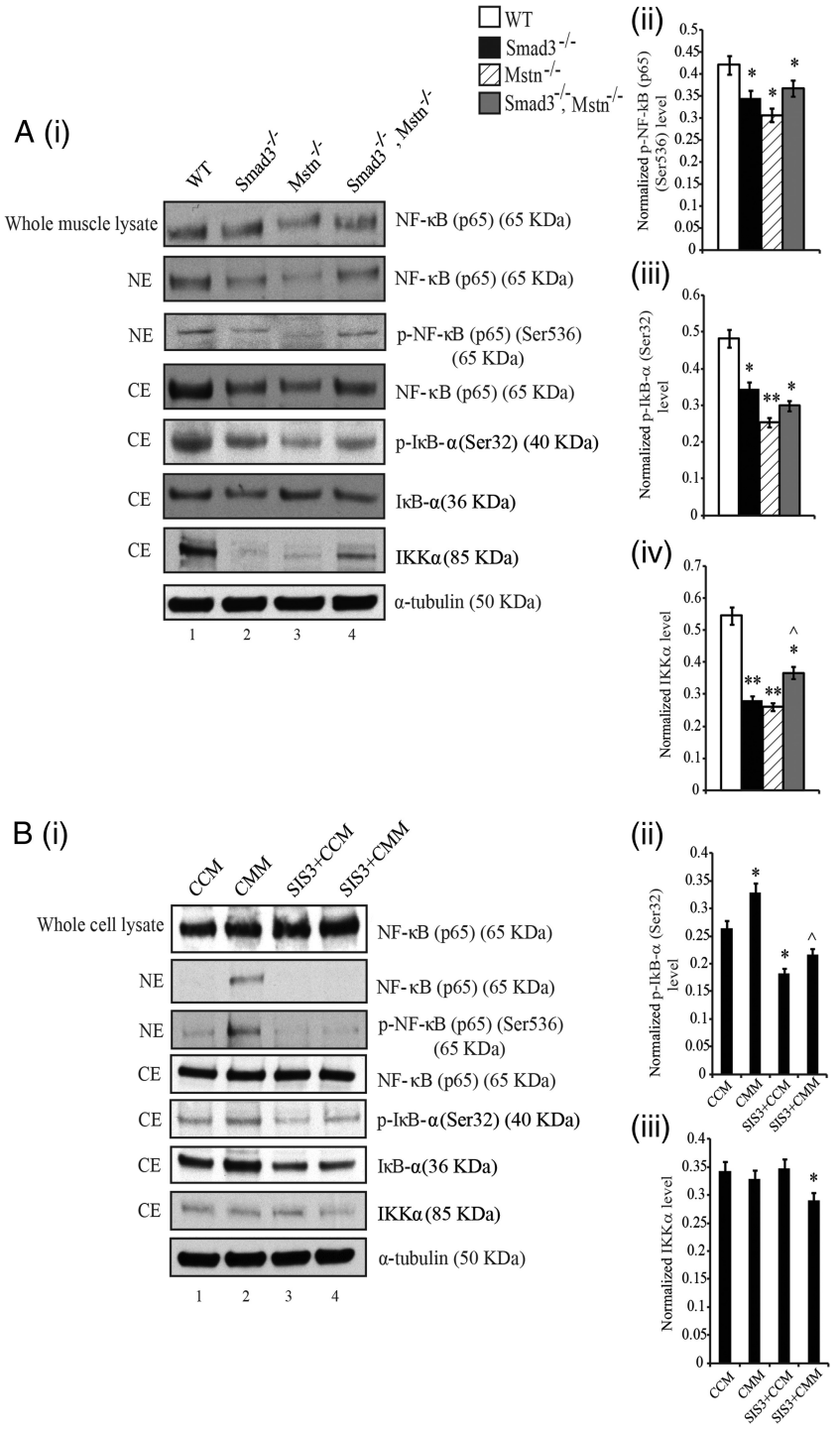

Figure 3. Smad3 is needed for IKKα-mediated activation of NF-κB (p65) by Mstn. A (i), Representative Western blot analysis of NF-κB (p65), p-NF-κB (p65), p-IκB-α, IκB-α, and IKKα protein levels in whole-muscle lysates, nuclear (NE) and cytoplasmic extracts (CE) obtained from biceps femoris muscle from WT (lane 1), Smad3$^{-/-}$ (lane 2), Mstn$^{-/-}$ (lane 3), and double-KO (lane 4) mice. Corresponding densitometric analysis of p-NF-κB (p65) (ii), p-IκB-α (iii), and IKKα (iv) protein levels. α-Tubulin was used as an internal control for equal protein loading on the gel. *, $P < .05$; **, $P < .01$: when compared to the WT muscle; ^, $P < .05$: when compared with Smad3$^{-/-}$ muscle (n = 3). B (i), Western blot analysis of NF-κB (p65), p-NF-κB (p65), p-IκB-α, IκB-α, and IKKα protein levels in whole-cell lysates, and nuclear (NE) and cytoplasmic extracts (CE) obtained from C2C12 cells treated with CCM (lane 1), CMM (lane 2), SIS3 and CCM (lane 3), and SIS3 and CMM (lane 4) for 48 hours during differentiation. Corresponding densitometric analysis of p-IκB-α (ii) and IKKα (iii) protein levels. α-Tubulin was used as an internal control for equal protein loading on the gel. *, $P < .05$: when compared with CCM-treated cells; ^, $P < .05$: when compared with CMM-treated cells (n = 2).

(Figure 3B(i), lanes 1 and 2, (ii), and (iii)). However, SIS3-mediated blockade of Smad3 prevented NF-κB (p65) activation even upon addition of CMM (Figure 3B (i), lanes 3 and 4, (ii), and (iii)). Similarly, Smad3 inhibition by short hairpin RNA also resulted in down-regulation of NF-κB (p65) signaling in shSmad3 C2C12 cells (Supplemental Figure 1). These data confirm that Smad3 is indispensable for Mstn-induced NF-κB-mediated ROS induction.

ROS is generated through MAPK pathways in Smad3$^{-/-}$ muscle

The results presented so far indicated that Mstn-mediated induction of ROS in Smad3$^{-/-}$ muscle occurs independently of NF-κB signaling. As such, we wanted to identify potential alternative signaling pathways through which Mstn may induce ROS production in the absence of Smad3. Previous studies have shown that Mstn can activate p38 MAPK through TGF-β-activated kinase 1 (TAK1) (15), c-Jun N-terminal kinase (JNK) (32), and/or ERK pathways (16). Hence, to determine whether p38 MAPK, JNK, and/or ERK pathways are involved in Mstn-mediated ROS production in the absence of Smad3, we probed for various downstream signaling molecules involved in these pathways in gastrocnemius muscle isolated from WT, Smad3$^{-/-}$, Mstn$^{-/-}$, and double-KO mice. As shown in Figure 4A and Supplemental Figure 2A(i), Smad3$^{-/-}$ muscle has higher levels of p-p38 MAPK (lane 2) when compared with WT muscle (lane 1), whereas Mstn$^{-/-}$ muscle (lane 3) and double-KO muscle (lane 4) have significantly lower levels of p-p38 MAPK. Total levels of p38 (Figure 4A) were significantly lower in WT and Smad3$^{-/-}$ muscle (lanes 1 and 2, respectively) and significantly higher in Mstn$^{-/-}$ and double-KO

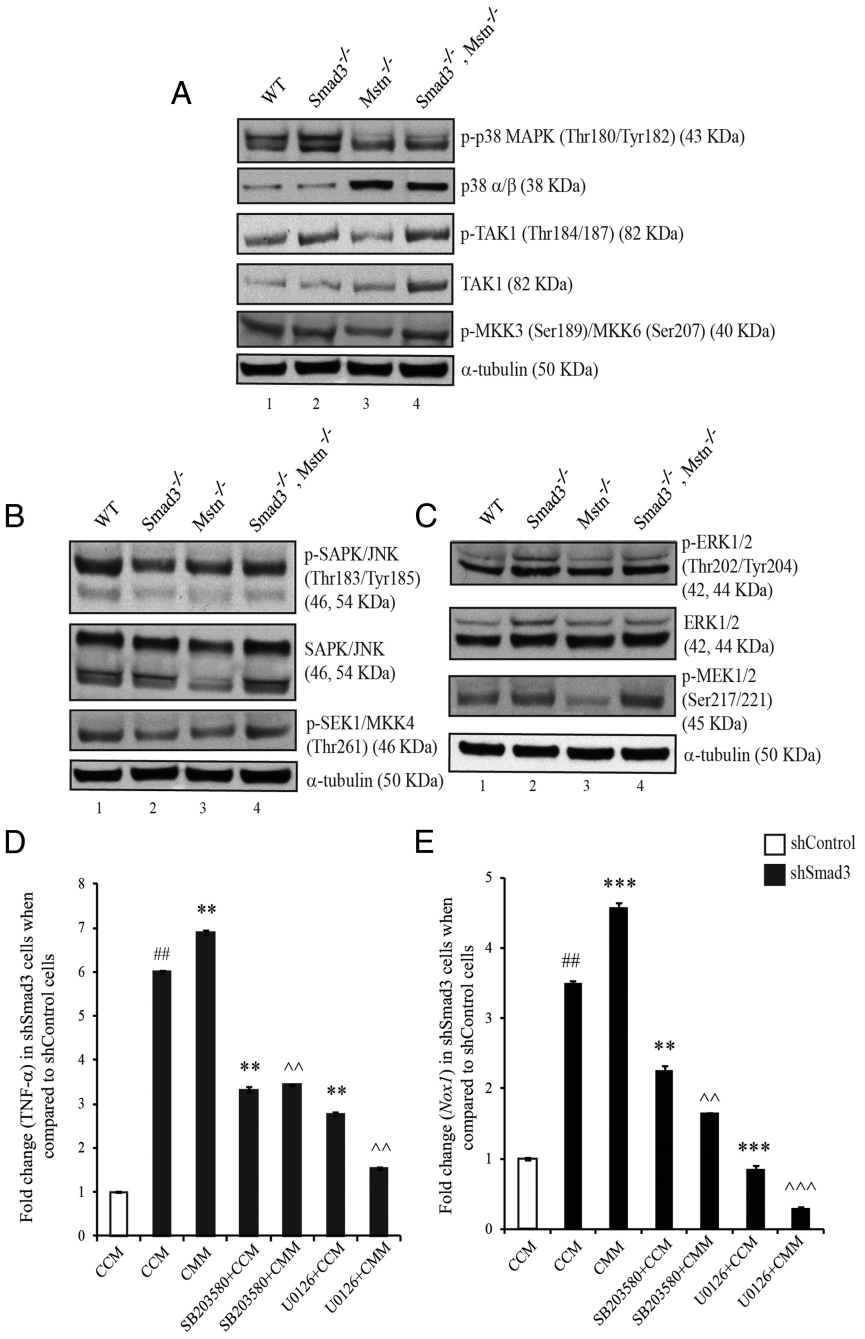

Figure 4. ROS is generated through p38 and ERK MAPK pathways in Smad3$^{-/-}$ muscle. Western blot analysis of p-p38 MAPK (A), p38 α/β (A), p-TAK1 (A), TAK1 (A), p-MKK3/6 (A), p-SAPK/JNK (B), SAPK/JNK (B), p-SEK1/MKK4 (B), p-ERK1/2 (C), ERK1/2 (C), and p-MEK1/2 (C) protein levels in protein lysates obtained from gastrocnemius muscle from WT (lane 1), Smad3$^{-/-}$ (lane 2), Mstn$^{-/-}$ (lane 3), and double-KO (lane 4) mice. α-Tubulin was used as an internal control for equal protein loading on the gels (n = 3). mRNA expression of TNF-α (D) and *Nox1* (E) in shSmad3 C2C12 cells pretreated for 2 hours with SB203580 or for 1 hour U0126 followed by 48-hour treatment with CCM or CMM in differentiation medium. The values are expressed as fold change when compared with respective shControl C2C12 cells. ##, $P < .01$: when compared with CCM-treated shControl C2C12 cells; **, $P < .01$; ***, $P < .001$: when compared with CCM-treated shSmad3 C2C12 cells; ^^, $P < .01$; ^^^, $P < .001$: when compared with CMM-treated shSmad3 C2C12 cells (n = 2). SAPK, stress-activated protein kinase.

muscle (lanes 3 and 4, respectively). To determine whether TAK1 plays a role in mediating Mstn-induced activation of p38, Western blot and densitometric analysis for p-TAK1 and total TAK1 was performed and results (Figure 4A and Supplemental Figure 2A(ii), respectively) indicated that p-TAK1 level was significantly increased in Smad3$^{-/-}$ and double-KO muscle (lanes 2 and 4, respectively) and significantly reduced in Mstn$^{-/-}$ muscle (lane 3), when compared with WT muscle (lane 1). An increase in total TAK1 level (Figure 4A and Supplemental Figure 2A(iii)) was observed in Mstn$^{-/-}$ (lane 3) and double-KO muscle (lane 4). Immunoblotting results for p-MKK3/6, which is a substrate of TAK1 and activator of p38, revealed that there was no significant change in the levels of p-MKK3/6 in Smad3$^{-/-}$ muscle (lane 2) and double-KO muscle (lane 4) when compared with the WT muscle (lane 1); however, lower levels of p-MKK3/6 were detected in Mstn$^{-/-}$ muscle (lane 3). These results indicate that Mstn activates p38 MAPK in the absence of Smad3 and that inactivation of Mstn downregulates the p38 MAPK activity in skeletal muscle.

Next we examined the contribution of the JNK pathway toward Mstn-mediated signaling in Smad3$^{-/-}$ mice. Western blot and subsequent densitometric analysis for p-JNK (Figure 4B and Supplemental Figure 2B(i), respectively) revealed that the levels of p-JNK were reduced in Smad3$^{-/-}$ (lane 2), Mstn$^{-/-}$ (lane 3), and double-KO (lane 4) muscle, when compared with WT muscle (lane 1). The level of p-MKK4, the kinase activator of JNK, was reduced in Smad3$^{-/-}$ (lane 2) and Mstn$^{-/-}$ (lane 3) muscle, whereas no significant difference was observed in double-KO muscle (lane 4), when compared with WT muscle (lane 1) (Figure 4B and Supplemental Figure 2B(ii)). These data revealed that there is reduced activity of the JNK pathway in the absence of Smad3 and Mstn in skeletal muscle.

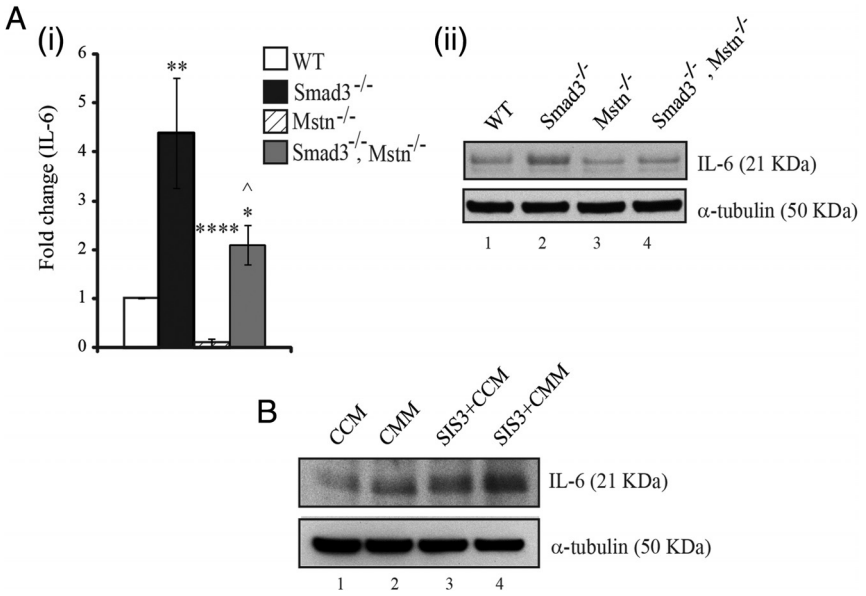

Figure 5. Absence of Smad3 led to the up-regulation of IL-6 in skeletal muscle. A (i), Representative graph showing mRNA expression of IL-6 in gastrocnemius muscle from WT, Smad3$^{-/-}$, Mstn$^{-/-}$, and double-KO mice. *, $P < .05$; **, $P < .01$; ****, $P < .0001$: when compared with the WT muscle; ^, $P < .05$: when compared with Smad3$^{-/-}$ muscle (n = 3). A (ii), Western blot analysis of IL-6 protein level in gastrocnemius muscle from WT (lane 1), Smad3$^{-/-}$ (lane 2), Mstn$^{-/-}$ (lane 3), and double-KO (lane 4) mice. α-Tubulin was used as an internal control for equal protein loading on the gel (n = 3). B, Western blot analysis of IL-6 protein in C2C12 myoblasts treated with CCM (lane 1), CMM (lane 2), SIS3+CMM (lane 3), and SIS3+CMM (lane 4) during differentiation for 48 hours. α-Tubulin was used as an internal control for equal protein loading on the gel (n = 2).

Lastly, we asked whether the ERK pathway was involved in Mstn signaling in Smad3$^{-/-}$ mice. Subsequent Western blot and densitometric analysis indicated that the levels of p-ERK1/2 and ERK1/2 (Figure 4C and Supplemental Figure 2C(i) and (ii), respectively) were higher in Smad3$^{-/-}$ muscle (lane 2) and in double-KO muscle (lane 4) when compared with WT muscle (lane 1). The p-ERK1/2 levels in double-KO muscle (lane 4) were slightly reduced when compared with Smad3$^{-/-}$ muscle (lane 2). In contrast, no significant difference was observed in the levels of p-ERK1/2 and total ERK1/2 in Mstn$^{-/-}$ muscle (lane 3). The level of p-MEK1/2 was increased in double-KO muscle (lane 4), relatively low in Mstn$^{-/-}$ muscle (lane 3), and showed no change in Smad3$^{-/-}$ muscle (lane 2) when compared with WT muscle (lane 1) (Figure 4C). These results indicate that ERK pathway is activated in Smad3$^{-/-}$ mice and that inactivation of Mstn partially rescues the activity of the ERK pathway.

To further confirm that MAPK pathways are involved in Mstn-mediated ROS production in the absence of Smad3, shControl and shSmad3 C2C12 were subjected to treatment with specific inhibitors of p38 MAPK (SB203580), JNK (SP600125), and ERK (U0126) signaling (Enzo Life Sciences, Inc), in the absence or presence of CMM during differentiation. The expression of TNF-α and *Nox1* was determined, and the results indicated that treatment with either SB203580 or U0126 significantly suppressed Mstn-mediated induction of TNF-α expression (Figure 4D) in shSmad3 C2C12 cells, whereas treatment with SP600125 only partially inhibited the Mstn-induced increase in TNF-α (our unpublished observations). Furthermore, all 3 inhibitors significantly suppressed the Mstn-induced increase in *Nox1* expression in shSmad3 C2C12 cells (Figure 4E). These results confirm that p38 MAPK and ERK pathways are involved in Mstn-mediated ROS production in Smad3$^{-/-}$ mice.

Absence of Smad3 led to the up-regulation of IL-6 in skeletal muscle

There has also been some evidence showing the relationship between MAPK pathways and IL-6 up-regulation (33, 34). IL-6 has been also shown to activate XO in endothelial cells (35) and skeletal muscle (36), resulting in the generation of ROS. Hence, the expression and protein level of IL-6 in the absence of Smad3 and/or Mstn was analyzed in gastrocnemius muscle from WT, Smad3$^{-/-}$, Mstn$^{-/-}$, and double-KO mice. The results show that the mRNA expression (Figure 5A(i)) and protein level (Figure 5A(ii)) of IL-6 was significantly up-regulated in Smad3$^{-/-}$ muscle (lane 2), significantly down-regulated in Mstn$^{-/-}$ muscle (lane 3), and partially rescued in double-KO muscle (lane 4), when compared with WT muscle (lane 1). In addition, treatment of C2C12 myoblasts with Mstn up-regulated IL-6 levels (lane 2), whereas treatment with SIS3 along with/without Mstn, further increased the IL-6 levels (lanes 3 and 4) (Figure 5B). These data suggest that Mstn up-regulates IL-6 in the absence of Smad3 whereas inactivation of Mstn can partially attenuate increased IL-6 expression.

CHOP-mediated MuRF1 up-regulation in Smad3$^{-/-}$ mice

Excess ROS have been demonstrated to induce Atrogin1 and MuRF1 (12, 37, 38), 2 important muscle-specific E3 ligases, and likewise these enzymes are up-regulated by Mstn (11, 12). However, in the absence of Smad3, MuRF1, but not Atrogin1, was up-regulated in

the skeletal muscle (quadriceps) (13). Moreover, previous results from our laboratory show that Smad3 signaling was dispensable for Mstn-mediated induction of MuRF1 (11). To further understand the molecular basis of differential expression of MuRF1 in Smad3$^{-/-}$ muscle, an in silico analysis was performed on the upstream sequences of the mouse *MuRF1* and *Atrogin1* promoter sequences to identify unique transcription factor-binding sites using the TFSEARCH tool (http://www.cbrc.jp/research/db/TFSEARCH.html). This analysis identified a putative CHOP-binding site (5′-GCAATGC-3′) within the *MuRF1* promoter, which was absent in Atrogin1 promoter. CHOP is an oxidative stress-induced transcription factor that further induces ROS and apoptosis in different cell types. To establish whether CHOP can activate *MuRF1* transcriptionally, C2C12 myoblasts were transfected with either pGL4.10 and pcDNA3 empty vectors or pGL4.10-*MuRF1* promoter construct (pGL4.10-MuRF1P) and pcDNA3 or pGL4.10-MuRF1P and pcDNA3-CHOP. Myoblasts transfected with pGL4.10-MuRF1P showed an approximately 2.0-fold increase in luciferase activity, when compared with myoblasts transfected with the empty vectors (Figure 6A). A further significant increase in luciferase activity was observed in myoblasts transfected with both CHOP expression vector (pcDNA3-CHOP) and pGL4.10-*MuRF1* promoter construct when compared with myoblasts transfected with pcDNA3 and pGL4.10-MuRF1P (Figure 6A). These results show that CHOP regulates *MuRF1* expression at the transcription level. Hence, to ascertain CHOP binding to *MuRF1* promoter sequence, EMSA was performed using nuclear extracts from WT and Smad3$^{-/-}$ biceps femoris muscle and the double-stranded oligonucleotides, bearing the CHOP binding site on the mouse *MuRF1* promoter (5′-AAAGTCTCAGT**GCAATGC**GCAGCCCATAA-3′). Smad3$^{-/-}$ muscles showed increased CHOP-binding activity indicated by the shifted band (lane 3) when compared with the WT muscle (lane 2) (Figure 6B(i)). To confirm the specificity of CHOP binding, nuclear extracts from WT and Smad3$^{-/-}$ biceps femoris muscle were preincubated with CHOP-specific antibody. As shown in Figure 6B(ii), our results showed diminished band intensity in nuclear extracts preincubated with CHOP antibody (lanes 4 and 5). Furthermore, when nuclear extracts were incubated with 500-fold concentration of competitor oligos, the disappearance of the shifted band was observed (Figure 6B(ii), lanes 6 and 7). To confirm the binding of CHOP on the *MuRF1* promoter in vivo, C2C12 cells were treated with SIS3 during differentiation and ChIP assay was performed. As shown in Figure 6C, enhanced binding of CHOP to the *MuRF1* promoter was observed in C2C12 cells upon SIS3 treatment (lane 8) when compared with the untreated cells (lane 7).

To investigate whether CHOP levels are altered in skeletal muscle of Smad3$^{-/-}$ mice, RT-qPCR and Western blot analysis for CHOP were performed in gastrocnemius muscle from WT, Smad3$^{-/-}$, Mstn$^{-/-}$, and double-KO mice. The results indicated that *Chop* mRNA expression (Figure 6D) and protein level (Figures 6E(i) and (ii)) was up-regulated in Smad3$^{-/-}$ muscles (lane 2). mRNA expression of *Chop* was up-regulated in Mstn$^{-/-}$ mice; however, no significant change was observed in CHOP protein levels in these mice (lane 3). *Chop* expression and level in double-KO muscle were similar to that of WT muscle (lane 4). Western blot analysis was also performed for MuRF1, and the results showed that MuRF1 levels were up-regulated in Smad3$^{-/-}$ muscle (lane 2) and reduced in Mstn$^{-/-}$ muscle (lane 3) and double-KO muscle (lane 4) (Figures 6E(i) and (ii)). Smad3 inhibition by SIS3 also showed significantly higher levels of CHOP in whole-cell lysates and nuclear and cytoplasmic extracts obtained from C2C12 myoblasts treated with SIS3 for 48 hours during differentiation (Figure 6F, lane 2). As expected, MuRF1 levels were increased upon SIS3 treatment (lane 2) when compared with the untreated myoblasts (Control) (lane 1) (Figure 6F). Collectively, these data confirm that elevated CHOP levels in the absence of Smad3 resulted in increased binding of CHOP to *MuRF1* promoter.

Discussion

Smad3 is required for normal skeletal muscle growth and development because lack of Smad3 leads to impaired myogenesis and skeletal muscle atrophy (13, 14). The pronounced muscle atrophy observed in Smad3$^{-/-}$ mice is due, in part, to the increased Mstn levels, because the inactivation of Mstn in Smad3$^{-/-}$ mice partially rescues the muscle atrophy seen in these mice (13). Previously, we have demonstrated that Mstn induces ROS production in skeletal muscle (12); therefore, we hypothesized that increased levels of Mstn in Smad3$^{-/-}$ muscle would lead to increased ROS. Indeed, our results show that Smad3$^{-/-}$ muscles display increased ROS levels and that Mstn is one of the key signaling factors behind the increased oxidative stress observed in these mice. In concurrence, inactivation of Mstn in Smad3$^{-/-}$ mice partially alleviated the oxidative stress.

Previous work has revealed that NF-κB is one of the downstream targets of Mstn (12) and Nox, mETC, and XO are well known downstream targets of NF-κB. However, our results indicated that ROS production was in-

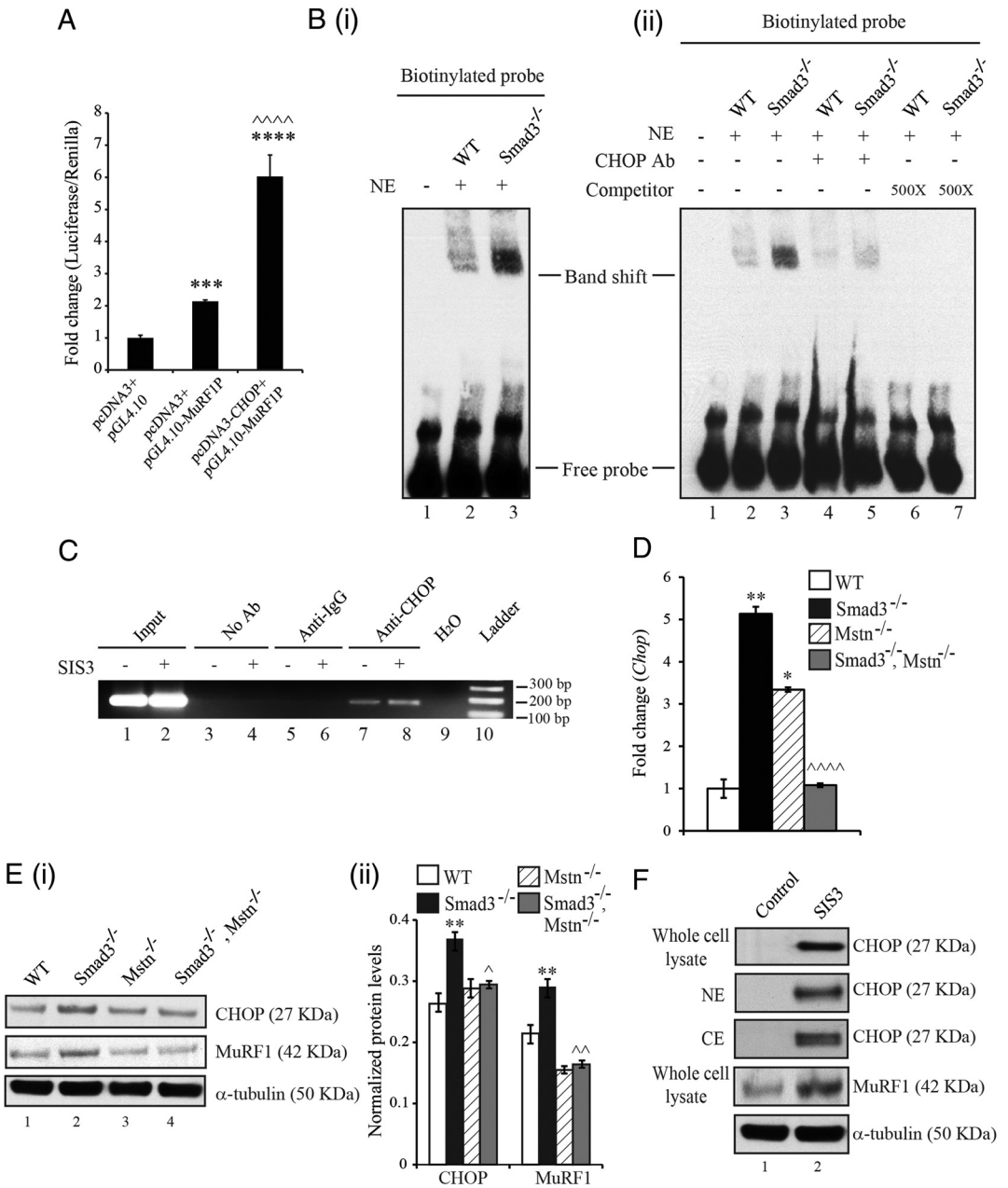

Figure 6. Enhanced binding of CHOP mediates MuRF1 up-regulation in Smad3$^{-/-}$ mice. A, Representative graph showing promoter-luciferase reporter activity in C2C12 myoblasts transfected with either pGL4.10 and pcDNA3 empty vectors or pGL4.10-MuRF1P and pcDNA3 or pGL4.10-MuRF1P and pcDNA3-CHOP, together with the control *Renilla* luciferase vector pRL-TK. (***, $P < .001$; ****, $P < .0001$: when compared with pGL4.10 and pcDNA3; ^^^^, $P < .0001$: when compared with pGL4.10-MuRF1P and pcDNA3; n = 3). B, EMSA was performed using nuclear extracts from WT and Smad3$^{-/-}$ biceps femoris muscle. (i) Left panel, representative gel showing increased CHOP binding in Smad3$^{-/-}$ muscle as indicated by the shifted band in lane 3 (lane 1, oligo only; lane 2, WT, Lane 3-Smad3$^{-/-}$). EMSA was also performed with nuclear extracts from WT and Smad3$^{-/-}$ biceps femoris muscle preincubated with CHOP-specific antibody. (ii) Right panel, representative gel showing the diminished band intensity of CHOP-specific band. Also, the disappearance of the shifted band in the nuclear extracts incubated with ×500 concentration of competitor oligos is observed. (lane 1,oligo only; lane 2, WT; lane 3, Smad3$^{-/-}$; lane 4,WT with CHOP antibody; lane 5, Smad3$^{-/-}$ with CHOP antibody; lane 6, WT with ×500 competitor oligos; lane 7,Smad3$^{-/-}$ with ×500 competitor oligos). C, Representative agarose gel image showing the binding of CHOP to *MuRF1* promoter (lanes 7 and 8), as assessed by ChIP, in C2C12 myoblasts treated with SIS3 for 48 hours during differentiation. The relative amounts of the input DNA in both untreated (lane 1) and SIS3 treated (lane 2) myoblasts were also assessed. Both no antibody (No Ab) (lanes 3 and 4) and isotype-specific IgG (lanes 5 and 6) controls are shown. D, Representative graph showing mRNA expression of *Chop* in gastrocnemius muscle from WT, Smad3$^{-/-}$, Mstn$^{-/-}$, and double-KO mice. *, $P < .05$; **, $P < .01$: when compared with the WT muscle; ^^^^, $P < .0001$: when compared with Smad3$^{-/-}$ muscle (n = 3). E, Western blot analysis (i) and densitometric analysis (ii) of CHOP and MuRF1 protein levels in gastrocnemius muscle from WT (lane 1), Smad3$^{-/-}$ (lane 2), Mstn$^{-/-}$ (lane 3), and double-KO (lane 4) mice. α-Tubulin was used as an internal control for equal protein loading on the gel; **, $P < .01$: when compared with the WT muscle; ^, $P < .05$; ^^, $P < .01$: when compared with Smad3$^{-/-}$ muscle (n = 3). F, Western blot analysis of CHOP protein levels in whole-cell lysates, nuclear (NE) and cytoplasmic extracts (CE), and MuRF1 levels in whole-cell lysates obtained from untreated C2C12 myoblasts (Control) (lane 1) and SIS3 treated (for 48 hours during differentiation) myoblasts (lane 2). α-Tubulin was used as an internal control for equal protein loading on the gel (n = 2). Ab, antibody.

dependent of NF-κB (p65) signaling in Smad3$^{-/-}$ muscle. Mstn has also been shown to signal through Smad2; therefore we also analyzed the phosphorylation of Smad2 (our unpublished observations). As expected Smad2 phosphorylation was enhanced in Smad3$^{-/-}$ muscle as well as in myoblasts with down-regulated Smad3. A point to note here is that despite increased phosphorylation of Smad2 and stimulation by Mstn, NF-κB (p65) signaling remained subdued in these muscles and myoblasts, suggesting the requirement of Smad3 for Mstn-mediated NF-κB (p65) signaling. However, inhibition of Smad2 alone in C2C12 cells (our unpublished observations) resulted in repression of basal levels of IKKα and NF-κB (p65), suggesting distinct roles of Smad2 and Smad3 in NF-κB (p65) signaling.

Considering the repression of NF-κB (p65) signaling in Smad3$^{-/-}$ muscle, we speculated that Mstn might be inducing ROS through transducers other than Smad2/3. Previously, the activation of p38 MAPK pathway by Mstn was shown to be independent of Smad3 signaling and resulted in inhibition of myoblast proliferation (15). Likewise, our data analysis revealed that in the absence of Smad3 (lane 2), p38 (via TAK1) and ERK MAPK pathways were up-regulated, and in double-KO mice (lane 4) there was a rescue of p38 and partial rescue of ERK pathway components (Figure 4, A and C). Also, Mstn-induced expression of TNF-α and *Nox1* in shSmad3 C2C12 cells, subjected to treatment with specific inhibitors of p38 MAPK (SB203580) and ERK (U0126) signaling, was significantly suppressed. These results confirm that p38 MAPK and ERK pathways are involved in Mstn-mediated ROS production in Smad3$^{-/-}$ mice.

IL-6 is a known inducer of ROS, and induction of IL-6 by Mstn via p38 MAPK pathway in skeletal muscle was seen previously (39). Our findings show that Smad3$^{-/-}$ mice have increased IL-6 levels (Figures 5A(i) and (ii)); moreover, Mstn induced IL-6 levels in C2C12 myoblasts (Figure 5B). IL-6 was also shown to be induced by ROS via p38 MAPK and ERK1/2 pathways in cardiac fibroblasts (33). Furthermore, IL-6 was induced by TNF-α (40), and our results show that Smad3$^{-/-}$ mice have increased expression of TNF-α. Thus, we propose that increased IL-6 in Smad3$^{-/-}$ muscle was due to an increase in TNF-α/MAPK signaling. The lower levels of IL-6 in Mstn$^{-/-}$ and double-KO mice can be accounted for by reduced MAPK signaling as well as lower levels of ROS, as indicated by reduced protein carbonylation (Figure 2A(i) and (ii)) and expression of TNF-α (Figure 2B) and *Nox1* (Figure 2C), found in these mice.

In an earlier report, IL-6 along with ROS was implicated in induc-

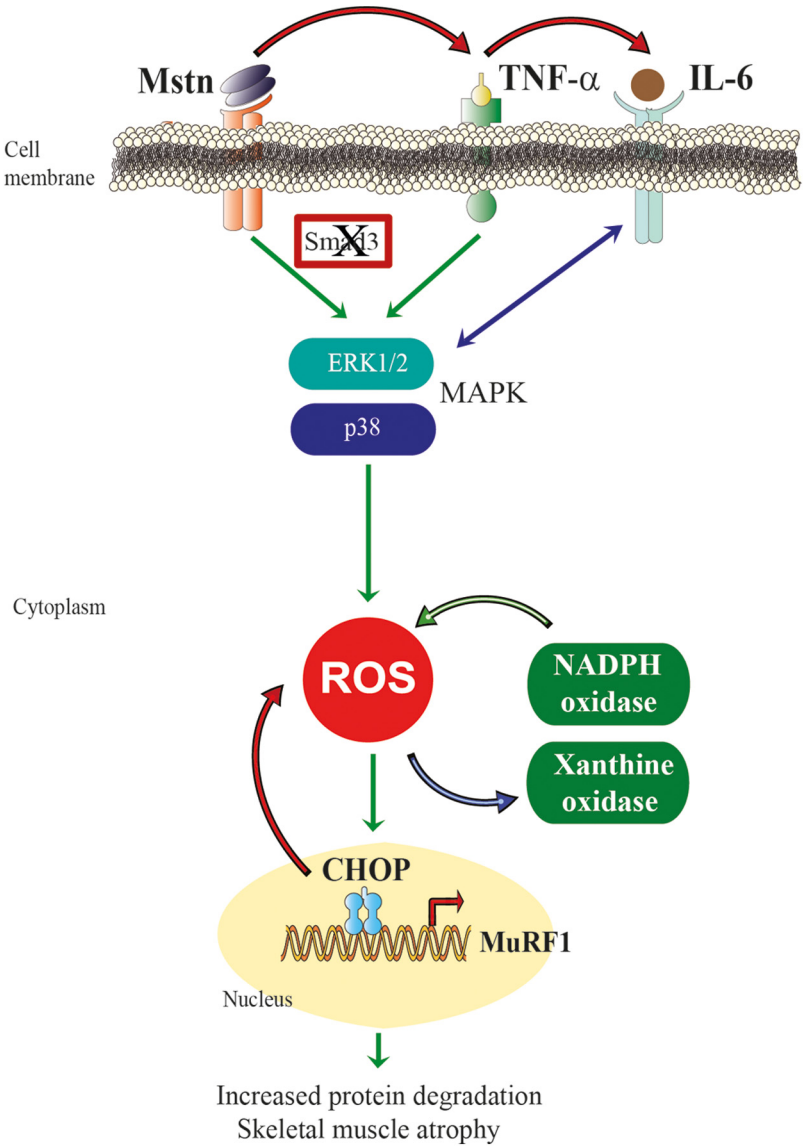

Figure 7. Proposed Smad3-independent mechanisms behind ROS production by Mstn. In the absence of Smad3, Mstn induces TNF-α and IL-6 to activate p38 and ERK MAPK to promote Nox- and XO-mediated induction of ROS. The excessive ROS leads to increased CHOP levels and up-regulation of *MuRF1* transcription. The increased CHOP protein levels also induce ROS production, and the enhanced ROS would further lead to increased Mstn production. NADPH, nicotinamide adenine dinucleotide phosphate.

ing XO activity (35, 36, 41). Consistently, our results show that Smad3$^{-/-}$ mice have increased XO activity. XO itself is a known source of ROS in tissues and generates ROS by catalyzing the oxidation of hypoxanthine and xanthine to uric acid. XO has also been shown to be activated by MAPK pathways, leading to increased ROS levels (42, 43). Altogether, our results suggest that in Smad3$^{-/-}$ mice, high levels of Mstn activate MAPK signaling cascades leading to up-regulation of IL-6, TNF-α, and XO to promote generation of ROS. As previously shown by us, ROS thus generated can stimulate Mstn production and thus maintain higher levels of ROS in the muscle (12).

Both Mstn and ROS have been demonstrated to up-regulate ubiquitination of proteins by E3 ligases like Atrogin1 and MuRF1 in skeletal muscle (11, 12). Because MuRF1 levels were up-regulated in Smad3$^{-/-}$ muscle, we speculated that expression/activity of various transcription factors that may be induced by oxidative stress or absence of Smad3 would be altered in these mice. Interestingly, an in silico analysis indicated a CHOP-binding site only on *MuRF1* promoter sequence and not on Atrogin1 promoter. CHOP is a stress-induced nuclear protein that is known to play a role in apoptosis, proliferation, differentiation, and oxidative stress (44–47). Indeed, activation of *MuRF1* promoter by CHOP indicated that CHOP is able to regulate the expression of *MuRF1* transcriptionally (Figure 6A). Further experiments confirmed that CHOP expression/level (Figure 6, D and E, (i) and (ii)) and binding to *MuRF1* promoter (Figure 6B(i) and (ii)) is indeed up-regulated in Smad3$^{-/-}$ muscle. SIS3-mediated inhibition of Smad3 in C2C12 myoblasts also increased binding of CHOP to *MuRF1* promoter as shown by ChIP assay (Figure 6C). Further, Mstn inactivation in Smad3$^{-/-}$ mice resulted in rescue of CHOP protein to WT levels. However, *Chop* expression was up-regulated in Mstn$^{-/-}$ mice (Figures 6D), suggesting that in Mstn$^{-/-}$ mice, CHOP could be regulated posttranscriptionally. An earlier report of p38 MAPK-mediated increase in CHOP activity (46) coincides with our results of enhanced p38 MAPK signaling and CHOP activity in Smad3$^{-/-}$ muscle. Moreover, CHOP has also been implicated to up-regulate IL-6 transcription (48), indicating the possibility of a role of CHOP in IL-6 regulation in Smad3$^{-/-}$ muscle as well.

Finally, we propose that in the absence of canonical Smad3 signaling, Mstn induces ROS through the activation of p38 and ERK MAPK pathways mediated via TNF-α, IL-6, Nox, and XO. The excessive ROS stimulated up-regulation of MuRF1 through CHOP, which eventually leads to muscle wasting in Smad3$^{-/-}$ muscle (Figure 7).

Acknowledgments

We thank Professor Se-Jin Lee (The Johns Hopkins University, Baltimore, MD) for providing Mstn$^{-/-}$ heterozygous mice. We are also thankful to Anuradha Vajjala, Zhi Hui Ng, Kelvin Tan Suan Liang, Sangiah Umamaheswari, Sushmitha Sathiyamoorthy, and Savitha Swaminathan for their help.

Address all correspondence and requests for reprints to: Mridula Sharma, Department of Biochemistry, YLLSoM, National University of Singapore, 14 Medical Drive, MD6, level 14 South Core, Singapore 117599. E-mail: bchmridu@nus.edu.sg.

This work was supported by CRP (to N.R.F.) and Tier1 and Tier2 (to M.O.E.), Singapore.

Disclosure Summary: The authors have nothing to disclose.

References

1. **Derynck R, Zhang YE.** Smad-dependent and Smad-independent pathways in TGF-β family signalling. *Nature*. 2003;425:577–584.
2. **Shi Y, Massagué J.** Mechanisms of TGF-β signaling from cell membrane to the nucleus. *Cell*. 2003;113:685–700.
3. **Fiocchi C.** TGF-β/Smad signaling defects in inflammatory bowel disease: mechanisms and possible novel therapies for chronic inflammation. *J Clin Invest*. 2001;108:523–526.
4. **Huang WC, Yen FC, Shie FS, et al.** TGF-β1 blockade of microglial chemotaxis toward Aβ aggregates involves SMAD signaling and down-regulation of CCL5. *J Neuroinflammation*. 2010;7:28.
5. **Bonniaud P, Margetts PJ, Ask K, Flanders K, Gauldie J, Kolb M.** TGF-β and Smad3 signaling link inflammation to chronic fibrogenesis. *J Immunol*. 2005;175:5390–5395.
6. **Liu D, Black BL, Derynck R.** TGF-β inhibits muscle differentiation through functional repression of myogenic transcription factors by Smad3. *Genes Dev*. 2001;15:2950–2966.
7. **Liu D, Kang JS, Derynck R.** TGF-β-activated Smad3 represses MEF2-dependent transcription in myogenic differentiation. *EMBO J*. 2004;23:1557–1566.
8. **Langley B, Thomas M, Bishop A, Sharma M, Gilmour S, Kambadur R.** Myostatin inhibits myoblast differentiation by down-regulating MyoD expression. *J Biol Chem*. 2002;277:49831–49840.
9. **Li ZB, Kollias HD, Wagner KR.** Myostatin directly regulates skeletal muscle fibrosis. *J Biol Chem*. 2008;283:19371–19378.
10. **McFarlane C, Hui GZ, Amanda WZ, et al.** Human myostatin negatively regulates human myoblast growth and differentiation. *Am J Physiol Cell Physiol*. 2011;301:C195–C203.
11. **Lokireddy S, McFarlane C, Ge X, et al.** Myostatin induces degradation of sarcomeric proteins through a Smad3 signaling mechanism during skeletal muscle wasting. *Mol Endocrinol*. 2011;25:1936–1949.
12. **Sriram S, Subramanian S, Sathiakumar D, et al.** Modulation of reactive oxygen species in skeletal muscle by myostatin is mediated through NF-κB. *Aging Cell*. 2011;10:931–948.
13. **Ge X, McFarlane C, Vajjala A, et al.** Smad3 signaling is required for satellite cell function and myogenic differentiation of myoblasts. *Cell Res*. 2011;21:1591–1604.
14. **Ge X, Vajjala A, McFarlane C, Wahli W, Sharma M, Kambadur R.** Lack of Smad3 signaling leads to impaired skeletal muscle regeneration. *Am J Physiol Endocrinol Metab*. 2012;303:E90–E102.
15. **Philip B, Lu Z, Gao Y.** Regulation of GDF-8 signaling by the p38 MAPK. *Cell Signal*. 2005;17:365–375.
16. **Yang W, Chen Y, Zhang Y, Wang X, Yang N, Zhu D.** Extracellular signal-regulated kinase 1/2 mitogen-activated protein kinase path-

way is involved in myostatin-regulated differentiation repression. *Cancer Res*. 2006;66:1320–1326.
17. **Zimmers TA, Davies MV, Koniaris LG, et al.** Induction of cachexia in mice by systemically administered myostatin. *Science*. 2002;296:1486–1488.
18. **McCroskery S, Thomas M, Maxwell L, Sharma M, Kambadur R.** Myostatin negatively regulates satellite cell activation and self-renewal. *J Cell Biol*. 2003;162:1135–1147.
19. **Partridge TA.** Tissue culture of skeletal muscle. *Methods Mol Biol*. 1997;75:131–144.
20. **Yaffe D, Saxel O.** Serial passaging and differentiation of myogenic cells isolated from dystrophic mouse muscle. *Nature*. 1977;270:725–727.
21. **Jinnin M, Ihn H, Tamaki K.** Characterization of SIS3, a novel specific inhibitor of Smad3, and its effect on transforming growth factor-β1-induced extracellular matrix expression. *Mol Pharmacol*. 2006;69:597–607.
22. **Baeza-Raja B, Muñoz-Cánoves P.** p38 MAPK-induced nuclear factor-κB activity is required for skeletal muscle differentiation: role of interleukin-6. *Mol Biol Cell*. 2004;15:2013–2026.
23. **Yu LY, Pei Y, Xia WB, Xing XP, Meng XW, Zhou XY.** Effect of fibroblast growth factor 9 on Runx2 gene promoter activity in MC3T3–E1 and C2C12 cells. *Chin Med J (Engl)*. 2007;120:491–495.
24. **Iuchi T, Akaike M, Mitsui T, et al.** Glucocorticoid excess induces superoxide production in vascular endothelial cells and elicits vascular endothelial dysfunction. *Circ Res*. 2003;92:81–87.
25. **Ye J, Cippitelli M, Dorman L, Ortaldo JR, Young HA.** The nuclear factor YY1 suppresses the human gamma interferon promoter through two mechanisms: inhibition of AP1 binding and activation of a silencer element. *Mol Cell Biol*. 1996;16:4744–4753.
26. **Bradford MM.** A rapid and sensitive method for the quantitation of microgram quantities of protein utilizing the principle of protein-dye binding. *Anal Biochem*. 1976;72:248–254.
27. **Bergmeyer HU.** *Methods of Enzymatic Analysis*. Vol 2. London and New York, NY: Academic Press; 1974.
28. **Beers RF Jr, Sizer IW.** A spectrophotometric method for measuring the breakdown of hydrogen peroxide by catalase. *J Biol Chem*. 1952;195:133–140.
29. **Rotruck JT, Pope AL, Ganther HE, Swanson AB, Hafeman DG, Hoekstra WG.** Selenium: biochemical role as a component of glutathione peroxidase. *Science*. 1973;179:588–590.
30. **Moron MS, Depierre JW, Mannervik B.** Levels of glutathione, glutathione reductase and glutathione S-transferase activities in rat lung and liver. *Biochim Biophys Acta*. 1979;582:67–78.
31. **Bonala S, Lokireddy S, Arigela H, et al.** Peroxisome proliferator-activated receptor β/δ induces myogenesis by modulating myostatin activity. *J Biol Chem*. 2012;287:12935–12951.
32. **Huang Z, Chen D, Zhang K, Yu B, Chen X, Meng J.** Regulation of myostatin signaling by c-Jun N-terminal kinase in C2C12 cells. *Cell Signal*. 2007;19:2286–2295.
33. **Sano M, Fukuda K, Sato T, et al.** ERK and p38 MAPK, but not NF-κB, are critically involved in reactive oxygen species-mediated induction of IL-6 by angiotensin II in cardiac fibroblasts. *Circ Res*. 2001;89:661–669.
34. **Aida Y, Honda K, Tanigawa S, et al.** IL-6 and soluble IL-6 receptor stimulate the production of MMPs and their inhibitors via JAK-STAT and ERK-MAPK signalling in human chondrocytes. *Cell Biol Int*. 2012;36:367–376.
35. **Wang G, Qian P, Jackson FR, Qian G, Wu G.** Sequential activation of JAKs, STATs and xanthine dehydrogenase/oxidase by hypoxia in lung microvascular endothelial cells. *Int J Biochem Cell Biol*. 2008;40:461–470.
36. **Hellsten Y, Frandsen U, Orthenblad N, Sjødin B, Richter EA.** Xanthine oxidase in human skeletal muscle following eccentric exercise: a role in inflammation. *J Physiol*. 1997;498:239–248.
37. **Li YP, Chen Y, Li AS, Reid MB.** Hydrogen peroxide stimulates ubiquitin-conjugating activity and expression of genes for specific E2 and E3 proteins in skeletal muscle myotubes. *Am J Physiol Cell Physiol*. 2003;285:C806–C812.
38. **Cai D, Frantz JD, Tawa NE, et al.** IKKβ/NF-κB activation causes severe muscle wasting in mice. *Cell*. 2004;119:285–298.
39. **Zhang L, Rajan V, Lin E, et al.** Pharmacological inhibition of myostatin suppresses systemic inflammation and muscle atrophy in mice with chronic kidney disease. *FASEB J*. 2011;25:1653–1663.
40. **Turner NA, Mughal RS, Warburton P, O'Regan DJ, Ball SG, Porter KE.** Mechanism of TNF-α-induced IL-1α, IL-1β and IL-6 expression in human cardiac fibroblasts: effects of statins and thiazolidinediones. *Cardiovasc Res*. 2007;76:81–90.
41. **Kosmidou I, Vassilakopoulos T, Xagorari A, Zakynthinos S, Papapetropoulos A, Roussos C.** Production of interleukin-6 by skeletal myotubes: role of reactive oxygen species. *Am J Respir Cell Mol Biol*. 2002;26:587–593.
42. **Abdulnour RE, Peng X, Finigan JH, et al.** Mechanical stress activates xanthine oxidoreductase through MAP kinase-dependent pathways. *Am J Physiol Lung Cell Mol Physiol*. 2006;291:L345–L353.
43. **Le A, Damico R, Damarla M, et al.** Alveolar cell apoptosis is dependent on p38 MAP kinase-mediated activation of xanthine oxidoreductase in ventilator-induced lung injury. *J Appl Physiol*. 2008;105:1282–1290.
44. **Alter J, Bengal E.** Stress-Induced C/EBP homology protein (CHOP) represses MyoD transcription to delay myoblast differentiation. *PLoS ONE*. 2011;6:e29498.
45. **Cao Z, Umek RM, McKnight SL.** Regulated expression of three C/EBP isoforms during adipose conversion of 3T3–L1 cells. *Genes Dev*. 1991;5:1538–1552.
46. **Maytin EV, Ubeda M, Lin JC, Habener JF.** Stress-inducible transcription factor CHOP/gadd153 induces apoptosis in mammalian cells via p38 kinase-dependent and -independent mechanisms. *Exp Cell Res*. 2001;267:193–204.
47. **Song B, Scheuner D, Ron D, Pennathur S, Kaufman RJ.** Chop deletion reduces oxidative stress, improves β cell function, and promotes cell survival in multiple mouse models of diabetes. *J Clin Invest*. 2008;118:3378–3389.
48. **Hattori T, Ohoka N, Hayashi H, Onozaki K.** C/EBP homologous protein (CHOP) up-regulates IL-6 transcription by trapping negative regulating NF-IL6 isoform. *FEBS Lett*. 2003;541:33–39.